Photonic Quantum Ring

J. C. Ahn, K. S. Kwak, B. H. Park, H. Y. Kang, J. Y. Kim, and O'Dae Kwon*

Department of Electronic and Electrical Engineering, Pohang University of Science and Technology, Pohang, 790-784, Korea

(Received 8 June 1998)

We report a quantum ringlike toroidal cavity naturally formed in a vertical-cavity-like active microdisk plane due to Rayleigh's band of whispering gallery modes. The $\sqrt{T}$-dependent redshift and a square-law property of microampere-range threshold currents down to 2 μA are consistent with a photonic quantum wire view, due to whispering gallery mode-induced dimensional reduction. [S0031-9007(98)08230-1]

PACS numbers: 42.55.Sa, 42.60.Da, 78.66.–w

For the last several years, there have been intensive developments of microdisk semiconductor lasers of whispering gallery (WG) modes for low-power and high-density photonic array applications. These efforts of earlier photopumped thumbtack-type WG lasers [1] have been evolving to photonic-wire lasers [2] and electropumped thumbtack-type WG lasers [3,4] of submilliampere threshold currents. In this Letter, we demonstrate a cylindrical vertical-cavity surface-emitting laser (VCSEL)-like diode that exhibits WG modes with unusual photonic quantum ring (PQR) characteristics such as μA-range threshold currents and spectral $\sqrt{T}$ dependence, in addition to the usual VCSEL mode. We will thus illustrate and analyze the two-threshold behavior of successive lasings, first the PQR and then the VCSEL as well. Indeed, the quantum wire behavior of the PQR is vividly demonstrated in the $\sqrt{T}$-dependent spectral peak shift data. We note that the quantum-ring-like WG modes are naturally formed in the circumferential Rayleigh band region [5] of the active microdisk of a regular multi-quantum-well VCSEL-like structure but without any intentional and real quantum ring patterning.

The PQR device differs from the previous WG lasers [1–4,6] in that the vertical confinement is improved by the top and bottom distributed Bragg reflector (DBR) layers, and that stripe or segmented top electrodes are used for vertical output coupling. The metal-organic vapor-phase epitaxy-grown device employs a 1λ thick active layer with four 80 Å $Al_{0.11}Ga_{0.89}As$ quantum wells (QWs), whose details have been described elsewhere [7–9]. In the active disk plane, the PQR region is defined by Rayleigh's bandwidth, $W_{\text{Rayleigh}} = (\phi/2)(1 - n_{\text{eff}}/n)$, where the WG mode occurs, which is well described in Ref. [10]: Rayleigh's annular band is defined by the active disk's radius $R(= \phi/2)$ for outer boundary and the inner reflection point $r_{\text{in}} = Rn_M/n$, where n is the refractive index of the active medium and n_M is the effective refractive index in azimuthal direction ($n_M \simeq n_{\text{eff}}$ [1]). The calculated profile of the annular WG emission based on Rayleigh's Bessel function analysis is shown in Fig. 1(a) for our device with $R = 7.5$ μm. The azimuthal mode number is rather large here, $M = 2\pi R n_{\text{eff}}/\lambda = 188$, and hence the 376 azimuthal peaks are not well distinguishable, unlike the intracavity axial VCSEL mode patterns being easily resolved as shown below. The exploded segment, Fig. 1(b), shows cross sectional details of the 1λ thick toroidal cavity of the PQR, formed by the vertical DBRs, together with the in-plane annular Rayleigh confinement, which then allows forward and backward helical wave propagations of the intratoroid WG modes, evanescently leading to the extracavity emission in radial direction [8].

We now illustrate unusual two-threshold successive lasing behaviors with the near-field micrographs of a 15-μm-diameter device as shown in Fig. 2. The annular PQR emission patterns in Figs. 2(a) and 2(b), exhibiting an onset of transparency of $\sim$3 μA and a threshold of $\sim$12 μA, respectively, correspond to the conventional WG lasers, which is extracavity evanescent field emission [1]. There occurs tremendous intensity buildup with increasing injection currents so that neutral density filters were used in taking pictures of Figs. 2(c) and 2(d). Nevertheless, the ring-shape emission pattern and spectral behaviors remain mostly unchanged. As the injection current increases above the second (VCSEL) threshold level of $\sim$12 mA, the emission of intra-VCSEL-cavity high-order transverse

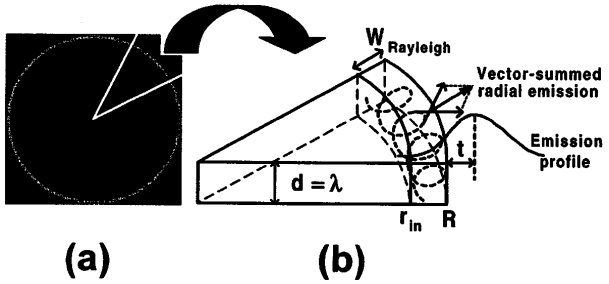

FIG. 1. Calculated WG mode ring. (a) Annular Rayleigh band with $R = 7.5$ μm, $W_{\text{Rayleigh}} = 0.36$ μm, and $M = 188$. Azimuthal maxima region generates the WG ring while all other ripples are filtered out with -9 dB cutoff in this plot. (b) An exploded segment shows the effective toroidal structure of the PQR, where R is the index-guided outer limit and r_{in} is the inner reflection limit which may also be reinforced by gain guiding. The radial evanescent field results from forward and backward helical traveling waves, and its intensity peaks at a distance $t \leq 1$ μm from the outer boundary.

 0031-9007/99/82(3)/536(4)$15.00

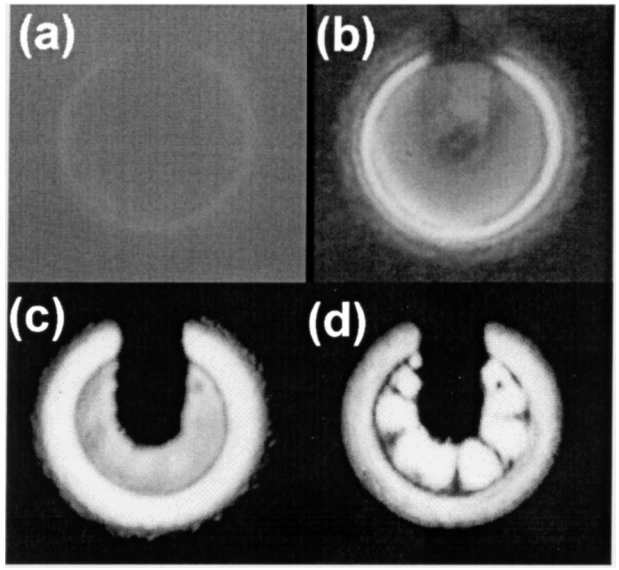

FIG. 2. Microscope pictures of the PQR laser. The emission is partly blocked due to the stripe electrode. (a) $I = 3\ \mu$A, where a faint evanescent mode image appears indicating the onset of the toroid transparency; (b) $I = 12\ \mu$A, near the PQR threshold; (c) $I = 11.5$ mA, right below the VCSEL threshold; (d) $I = 12$ mA, at the VCSEL threshold.

axial mode with 10-fold rotational symmetry appears [9]. We also note that, after the VCSEL threshold, the mode energies in the toroidal cavity split into intracavity VCSEL mode and extracavity PQR WG modes, and that recent studies of ultralow threshold VCSELs may have to consider this mode split loss.

We now mention some previous reports [11,12] of observing WG modes from VCSEL structures with distinguishable azimuthal peak patterns, even though the observed WG mode patterns, sizewise, seem to be rather intracavitylike. However, since the reports never discuss the temperature dependence as described below, a direct comparison with our results is impossible. Otherwise, perhaps due to submicron azimuthal mode spacings, there has been no report of distinguishable WG patterns actually observed [1,4].

The room temperature CW light-current data for the PQR device in Fig. 3 were collected by reading spectral peak intensities that become resolvable for $I > 400\ \mu$A with a microprobe made of a tapered single mode fiber and a spectrum analyzer (HP model 70951A). After the VCSEL threshold, the portion of curve for the PQR emission was not separable from that of the VCSEL, because of data overlapping due to a monitoring microscope placed right above the device. The near-vertical PQR emission, with an off-normal probe angle of $\sim 5°$, had a spectral linewidth of ~ 0.5 nm as compared with the VCSEL linewidth of ~ 0.2 nm. The broadened PQR linewidth due to peripheral surface roughness will be discussed later.

To distinguish the PQR WG mode from the VCSEL mode, we present the wavelength shift data for both as a function of the device temperature in Fig. 4 [13].

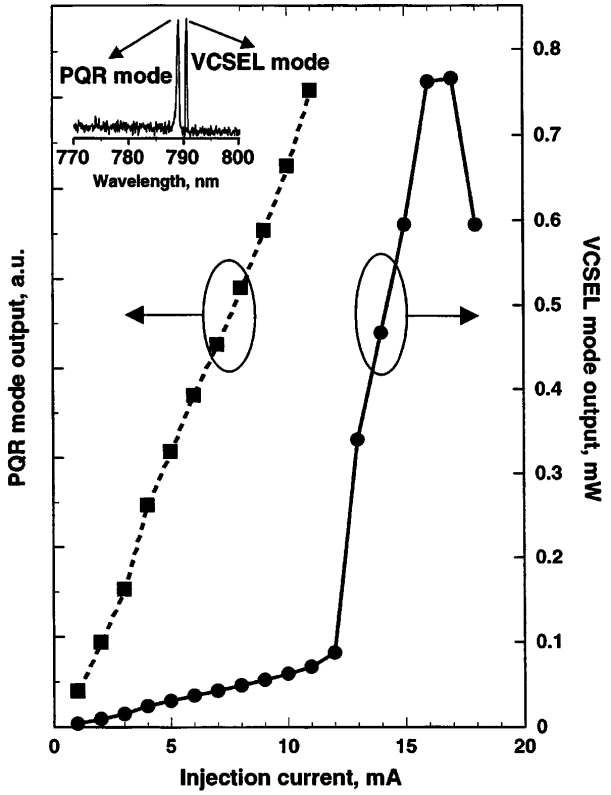

FIG. 3. Light-current curves of the PQR and VCSEL modes. We note that data fluctuations occur in the low current region especially for the PQR spectral peak measurements. The microprobe for PQR measurements had a collection efficiency of $\sim 20\%$ within a given radial segment. The inset shows typical spectra, at $I = 5$ mA for PQR and at 13 mA for VCSEL.

It is notable that the spectral shift of the PQR mode shows a distinct $\sqrt{T}$ dependence, while the VCSEL mode wavelength increases linearly at a rate of 0.07 nm/°C. The best fits to both curves in Fig. 4 are given as $\lambda_{\mathrm{PQR}} = 0.42\sqrt{T - 18} + 794.3$ [nm] and $\lambda_{\mathrm{VCSEL}} = 0.07T + 794.3$ [nm], respectively. One of the results in Ref. [14] shows linear T dependence for both the index-dominated

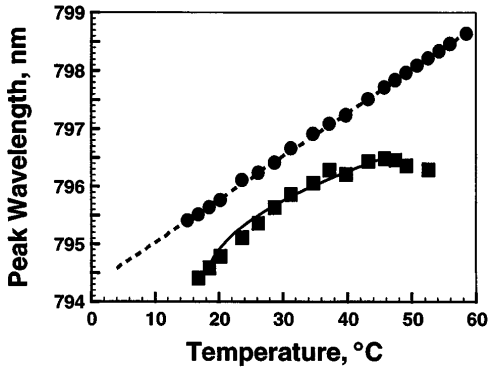

FIG. 4. Temperature dependent spectra measured with a constant injection current, $I = 12$ mA. Circles represent spectral data for the VCSEL, while squares are for the PQR, indicating a $\sqrt{T}$ dependence.

spectral change for short resonant cavities like the VCSEL and the gain-dominated spectral change for long cavities like the edge-emitting diode. The previously measured temperature coefficient of 0.07 nm/°C for the intracavity VCSEL mode is consistent with the index-dominated mechanism. On the other hand, the three-dimensional Rayleigh toroid for the PQR emission is to be classified as a long cavity confining the helical wave propagation along the circumference of the active disk, and hence the PQR emission ought to be gain dominated. The observed spectral $\sqrt{T}$ dependence then implies a gain-induced lasing, and is best explained by the quantum wire assumption, i.e., $\sqrt{T}$-dependent transparency condition [15].

We now pay special attention to the $\sqrt{T}$-dependent characteristics of the PQR because the PQRs would occupy the peripheral region of the four QW active disk, which should have a uniform carrier distribution. However, the observed two-threshold emission behavior indicates a significantly lowered transparency level for the PQR region as seen in Fig. 2(a), compared with that of the central region of the QW plane. A possible reason for this is the Rayleigh confinement mechanism leading to the three-dimensional toroidal cavity. This peculiar confinement appears to limit the number of guided resonant modes drastically, which in turn reduces the amount of energy required for the overall PQR mode excitation. Moreover, the above situation may involve a possible universal mechanism of dimensional reduction [16], and is also effectively analogous to the enhancement of the spontaneous emission factor β, which is the key interest of the various microcavity structures suggested such as microdisk, microdroplet, and photonic band gap structures [17]. We also note that wavelength shifts of the PQR mode level off in the region of $T \geq 40$ °C, which might solve the nagging problem of the spectral wandering due to local device heating associated with typical high-density laser arrays.

The Rayleigh toroid, associated with the PQR emission as described above, is to confine the WG modal manifolds of the above-mentioned helically twisted traveling waves. We thus propose a concept of two-dimensional pseudoquantum rings for providing carriers needed for the excitation of the WG modal manifolds, which would take place well below the transparency of the whole QW plane [18]. In order to estimate the threshold current of the WG emission, we now assume the toroidal structure of our device as a concentric array of PQRs whose lateral characteristic unit length is defined by half the wavelength ($\lambda_{\mathrm{PQR}}/2$), being much larger than de Broglie's wavelength, to reflect the nature of paraxial light wave characterized by transverse peaks with a half-cycle interval. For such a pseudoquantum wire, assumed to provide the carriers needed for the individual PQR, the transparency carrier density is calculated by using a formula [15], $N_{\mathrm{tr}} = (\sqrt{2m_C}/\pi\hbar) \times 1.072\sqrt{k_B(T + 273)}$. The overall transparency current, $I_{\mathrm{tr}}^{\mathrm{Rayleigh}}$, can now be calculated by multiplying the transparency current, $I_{\mathrm{tr}}^{\mathrm{PQR}} = N_{\mathrm{tr}}\pi\phi e/\eta\tau$, for a single quantum-wire ring with the number (χ) of concentric rings within the active Rayleigh WG band so that $I_{\mathrm{tr}}^{\mathrm{Rayleigh}} \equiv \chi I_{\mathrm{tr}}^{\mathrm{PQR}} = W_{\mathrm{Rayleigh}}/(\lambda_{\mathrm{PQR}}/2n_{\mathrm{eff}})(N_{\mathrm{tr}}\pi\phi e/\eta\tau)$, where ϕ is the device diameter, η the quantum efficiency, and τ the carrier lifetime. The additional terms [15] due to the intrinsic loss $\alpha_i = 5\ \mathrm{cm}^{-1}$ [19] and the mirror loss are then included in the final expression for the threshold current:

$$
\begin{aligned}
I_{th} &= I_{\mathrm{tr}}^{\mathrm{Rayleigh}} + I_i + I_{\mathrm{mirror}} \\
&= \left(\frac{\pi n_{\mathrm{eff}} e N_{\mathrm{tr}} w}{\lambda_{\mathrm{PQR}}\tau}\right)\phi^2 + \left(\frac{\pi de\alpha_i w}{2g'_{1\mathrm{D}}\tau}\right)\phi^2 \\
&\quad + \left(\frac{dew \ln R^{-1}}{2g'_{1\mathrm{D}}\tau}\right)\phi\,, \qquad (1)
\end{aligned}
$$

where $w \equiv 1 - n_{\mathrm{eff}}/n = W_{\mathrm{Rayleigh}}/R$ is a normalized Rayleigh bandwidth, d is the active region thickness, and $g'_{1\mathrm{D}} = 8 \times 10^{-16}\ \mathrm{cm}^2$ [19] is the differential gain coefficient. This formula indicates a square-law property, $I_{th} \propto \phi^2$, excluding the relatively small contribution from the DBR mirror loss. A comparison between experiment and theory is shown in Fig. 5, and it indeed suggests an excellent agreement except some systematic discrepancies presumably due to substantial scattering losses associated with microscopically rough peripheral structures [8]. As the device diameter decreases, the Rayleigh bandwidth W_{Rayleigh} also decreases, and in turn the scattering loss due to the peripheral surface roughness is now more serious and thus becomes the dominant loss factor. This loss affects the observed threshold currents: for instance, $I_{th} = 2\ \mu$A, larger than the calculated value $I_{th} = 0.8\ \mu$A for $\phi = 6\ \mu$m, as tabulated in Fig. 5. The peripheral roughness is also related to the broad linewidth of the PQR mode, 0.5 nm, which is relatively large compared with the VCSEL linewidth. Refined epitaxy, lithography, and etching processes [9] for smoother cylindrical surface, minimizing the scattering loss [1,4], will further narrow the linewidth of the PQR emission like that of VCSELs.

In summary, we have observed ultralow threshold currents of $\sim\mu$A range, and two-threshold successive lasings

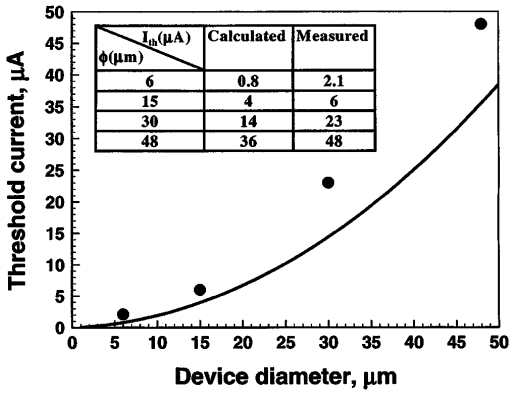

ϕ(μm) \ I_{th}(μA)	Calculated	Measured
6	0.8	2.1
15	4	6
30	14	23
48	36	48

FIG. 5. Size-dependent PQR threshold currents. The solid curve is from Eq. (1), and the circles are from PQR threshold currents measured.

of the PQR and VCSEL modes, from a toroidal cavity naturally formed in a VCSEL-like microcavity structure. We have also shown the $\sqrt{T}$ dependence of the spectral peak shift and a square-law behavior of threshold currents, consistent with the PQR analysis. Further work for lowered scattering loss is also under way for achieving linewidth-narrowed, submicroampere laser diodes so that the high-density integration of photonics to electronics become a reality.

The authors thank Dr. R. E. Slusher, Dr. D. A. B. Miller, and Dr. L. M. F. Chirovsky for helpful discussions, and H. Han, H. K. Shin, and B. S. Yoo for technical assistance. This work was supported by KT, Samsung Co., and KOSEF and ADD through KAIST.

*Email address: odkwon@postech.ac.kr

[1] S. L. McCall, A. F. J. Levi, R. E. Slusher, S. J. Pearton, and R. A. Logan, Appl. Phys. Lett. **60**, 289 (1992).

[2] J. P. Zhang, D. Y. Chu, S. L. Wu, S. T. Ho, W. G. Bi, C. W. Tu, and R. C. Tiberio, Phys. Rev. Lett. **75**, 2678 (1995).

[3] A. F. Levi, R. E. Slusher, S. L. McCall, T. Tanbun-Ek, D. L. Coblentz, and S. J. Pearton, Electron. Lett. **23**, 1010 (1992).

[4] T. Baba, M. Fujita, A. Sasaki, M. Kihara, and R. Watanabe, IEEE Photonics Technol. Lett. **9**, 878 (1997).

[5] Lord Rayleigh, *The Problem of the Whispering Gallery*, Scientific Papers Vol. 5 (Cambridge University, Cambridge, England, 1912), pp. 617–620.

[6] I. Ury, S. Margalit, N. Bar-chaim, M. Yust, D. Wilt, and A. Yariv, Appl. Phys. Lett. **36**, 629 (1980); A. F. Levi, R. E. Slusher, S. L. McCall, S. J. Pearton, and W. S. Hobson, Appl. Phys. Lett. **62**, 2021 (1993).

[7] O'Dae Kwon, J. C. Ahn, and H. Y. Kang, postdeadline paper to the Technical Digest OECC'97, Seoul, Korea, 1997, pp. 6 and 7, paper PDP1-3.

[8] J. C. Ahn, H. Y. Kang, and O'Dae Kwon, in *Optoelectronics '98*, SPIE Proceedings Vol. 3283 (SPIE-International Society for Optical Engineering, Bellingham, WA, 1998), pp. 241–251.

[9] J. C. Ahn, H. Y. Kang, N. J. Son, B. H. Park, K. S. Kwak, Y. H. Lee, and O'Dae Kwon, Jpn. J. Appl. Phys. **36**, 2134 (1997). High-order transverse VCSEL modes here showed T-dependent spectra as well; S. W. Lee, K. U. Chu, S. W. Kim, S. Park, O'Dae Kwon, K. W. Goossen, and S. S. Pei, Appl. Phys. Lett. **64**, 3065 (1994).

[10] M. K. Chin, D. Y. Chu, and S. T. Ho, J. Appl. Phys. **75**, 3302 (1994).

[11] D. Arbel, L. Djaloshinski, and M. Orenstein, in Digest of the 15th IEEE International Semiconductor Laser Conference (IEEE, Piscataway, NJ, 1996), p. 79; L. Djaloshinski and M. Orenstein, Opt. Lett. **23**, 364 (1998).

[12] H. Deng, Q. Deng, and D. G. Deppe, Appl. Phys. Lett. **69**, 3120 (1996); Q. Deng, H. Deng, and D. G. Deppe, Opt. Lett. **22**, 463 (1997).

[13] Details of temperature experiments will be published elsewhere.

[14] G. W. Taylor and P. A. Evaldsson, IEEE J. Quantum Electron. **QE-30**, 2262 (1994).

[15] A. Yariv, Appl. Phys. Lett. **53**, 1033 (1988).

[16] For an example in the two dimensions of the QW plane with a uniform carrier distribution, we may have a dynamically generated carrier concentration hump, a quantum-wire-like one-dimensional nature, along the peripheral boundary. This is analogous to the soaring water head at the moment of a collision with the wall of a pier as the waves rush and collapse.

[17] H. Yokoyama and S. D. Brorson, J. Appl. Phys. **66**, 4801 (1989); Y. Yamamoto and R. E. Slusher, Phys. Today **46**, No. 6, 66 (1993); *Optical Processes in Microcavities*, edited by R. K. Chuang and A. J. Campillo (World Scientific, Singapore, 1996), Chap. 10.

[18] We have recently found that hollow cylindrical cavities show similar PQR threshold characteristics as well. This aspect will be reported elsewhere.

[19] P. S. Zory, *Quantum Well Lasers* (Academic, San Diego, 1993).